UCRL-JRNL-225453

LAWRENCE
LIVERMORE
NATIONAL
LABORATORY

Orbital HP-Clouds for Solving Schrödinger Equation inQuantum Mechanics

J.S. Chen, W. Hu, M.A. Puso

October 20, 2006

Orbital HP-Clouds for Solving Schrödinger Equation in Quantum Mechanics

J. S. Chen[1], W. Hu[2], M. Puso[3]

Abstract

Solving Schrödinger equation in quantum mechanics presents a challenging task in numerical methods due to the high order behavior and high dimension characteristics in the wave functions, in addition to the highly coupled nature between wave functions. This work introduces orbital and polynomial enrichment functions to the partition of unity for solution of Schrödinger equation under the framework of HP-Clouds. An intrinsic enrichment of orbital function and extrinsic enrichment of monomial functions are proposed. Due to the employment of higher order basis functions, a higher order stabilized conforming nodal integration is developed. The proposed methods are implemented using the density functional theory for solution of Schrödinger equation. Analysis of several single and multi-electron/nucleus structures demonstrates the effectiveness of the proposed method.

Keywords: Partition of unity, HP-Clouds, Nodal integration, Schrödinger equation, Quantum mechanics

---

[1] *Corresponding Author, Professor, Department of Civil and Environmental Engineering, University of California, Los Angeles, Los Angeles, CA 90095-1593, USA*
[2] *Department of Civil and Environmental Engineering, University of California, Los Angeles, Los Angeles, CA 90095-1593, USA*
[3] *Department of Mechanical Engineering, Lawrence Livermore National Laboratory, Livermore, California, USA*

1. Introduction

During the last few decades, first principle calculation for electronic structures is primarily performed using basis set calculation under *ab initio* framework. A number of basis functions have been constructed and used for different quantum systems, such as Gaussian type orbital functions (GTOs) and Slater type orbital functions (STOs) in traditional *ab initio* calculation [26], and plane-wave orbital functions (PW) for density functional theory [29,44]. GTOs and STOs are commonly used for the small- and medium-sized atoms and molecules [53]. The advantage of using these orbital functions is that all of the integrals for computing the Hamiltonian matrix elements can be done analytically. However, these orbital basis functions are global functions, which yield a full sized Hamiltonian matrix [51]. PW functions are efficient for density functional theory, especially for crystal structures [44]. Nevertheless, the resolution of PW can not be controlled locally, thus a very large number of PW functions are needed globally in order to obtain reliable solution near the atomic core. Further, PW approach can only deal with periodic boundary conditions, which is not desirable for molecular systems.

Finite difference method (FDM) [1,14,15] and finite element method (FEM) [27,28,43,44,49, 50,51,53,54,55] have also been introduced in real-space *ab initio* calculation, but they require large degrees of freedom for reasonable accuracy. Pickett [44] introduced FEM for computing all-electron and pseudo-potential formulations under density functional theory. Tsuchida et al. [50] proposed an efficient scheme by introducing adaptive curvilinear coordinates into FEM to vary the grid logarithmically near the nuclei for accurate representation of wave functions. Recently, Yamakawa et al. [54,55] introduced Gaussian-FEM to enrich standard FEM with special GTOs orbital basis functions to increase the accuracy in describing the core electron, which, however, makes the approximation global.

Meshfree methods developed in the last two decades [2, 4,9,11,16,19,22,25,33,35,39,41,46,47] offer several unique features that are difficult to achieve in the conventional FEM. This class of methods employs approximation functions that are constructed entirely based on a set of scattered points. Compatibility requirement in FEM shape function is usually unnecessary in meshfree methods and thus they offer considerable simplicity in performing adaptive refinement [22,23,24,32,37,40,56] and in introducing special enrichment functions for enhanced solution accuracy [10,11]. Enrichment methods introduced in meshfree formulation can be classified in two types, the intrinsic and extrinsic enrichments [8]. Examples of intrinsic enrichment are the moving least-squares approximation [9,31] and reproducing kernel approximation [33]. These approximations introduce reproducibility of basis functions. The advantage of intrinsic enrichment is that no additional global degrees of freedom are needed with enrichment, however, enlarged non locality is required and discontinuity in the approximated function exists when enrichment functions vary in space even if they are C^∞ functions. The extrinsic enrichment, on the other hand, requires additional global degrees of freedom. Nevertheless, the discontinuity problem in the adaptive intrinsic enrichment does not exist when different extrinsic enrichment functions are used at different discrete points. Generalized finite element method [3,5,21,34] and eXtended finite element method [38] introduce extrinsic enrichment to the finite element approximation. An extrinsic enrichment of an interface enrichment function for composite materials has also been proposed [52]. Combined intrinsic and extrinsic enrichment can be formulated based on partition of unity [4,6,34,35,36] under the framework of HP-Clouds

[22,23,24,32,37,40]. In this work we introduce orbital intrinsic enrichment function and monomial extrinsic enrichment functions of partition of unity under HP-Clouds framework for solving Schrödinger equation in quantum mechanics.

Domain integration is an important task in meshfree method constructed based on Galerkin weak form. Gauss quadrature rules are commonly used in the early development of meshfree methods [9,33]. However, using quadrature rules on integration cells results in considerable integration error when the integration cells do not match with the support regions of shape function [20]. Sufficiently higher order quadrature rules and fine integration cells are usually used to reduce the integration error, leading to high computational cost. An alternative approach to simplify domain integration is to integrate weak form at nodal points. Although computationally efficient, direct nodal integration yields a rank deficiency and low accuracy. Several methods have been introduced as a correction and stabilization of nodal integration. Beissel et al. [7] proposed a least-squares stabilization technique. Randles et al. [45] introduced stress point method to enhance collocation formulation for SPH. Bonet et al. [12] presented a correction term into the derivative of shape function at nodal point. Chen et al. [17,18] proposed a stabilized conforming nodal integration (SCNI) as a stabilization of rank instability in nodal integration, and as a mechanism to pass linear patch test. In this work we introduce a higher order extension of SCNI for the proposed orbital HP-Clouds.

This paper is organized as follows. We first give an overview of basic Schrödinger equation in quantum mechanics in Section 2. In Section 3, we present an HP-Cloud approximation based on partition of unity with orbital intrinsic enrichment and monomial extrinsic enrichment. In Section 4, we construct discrete equation for Schrödinger equation using the proposed orbital HP-Cloud approximation, and introduce a higher order stabilized conforming nodal integration for Schrödinger equation. In Section 5, we solve several quantum systems using the proposed methods and compare the solution with those obtained by finite element methods. Concluding remarks are given in Section 6.

2. Schrödinger Equation in Quantum Mechanics

The motion of particles in quantum scale exhibits some abnormal characteristics, for example, electron diffraction in the experiment of G. P. Thomson, which violates the principles in classical mechanics [13]. Probability wave function $\overline{\varPsi}$ has been introduced to describe the motion of particles by the assumption of wave-particle duality. Wave function includes all the information of the quantum system, and the momentum operator $\hat{p}$, kinetic energy operator $\hat{T}$, and Hamiltonian operator $\hat{H}$ acting on the wave function $\overline{\varPsi}$ yield corresponding physical quantities that can be used to describe the particle motion [13].

The most fundamental equation in quantum mechanics is the Schrödinger equation that governs the wave function based on energy conservation:

$$\hat{H}\left(\mathbf{r}_1,\mathbf{r}_2,\ldots,\mathbf{r}_N,t\right)\overline{\varPsi}\left(\mathbf{r}_1,\mathbf{r}_2,\ldots,\mathbf{r}_N,t\right)=i\hbar\frac{\partial}{\partial t}\overline{\varPsi}\left(\mathbf{r}_1,\mathbf{r}_2,\ldots,\mathbf{r}_N,t\right) \tag{1}$$

where $\mathbf{r}_i$ is the position vector of the i-th particle, N is the total number of particles, $i\hbar\dfrac{\partial}{\partial t}$ is total energy operator, i is the imaginary unit, and $\hbar$ is the Plank constant. In the case where the potential field is time-independent, that is, the Hamiltonian operator is time-independent, the static Schrödinger equation for atomic/molecular systems can be derived from equation (1) by taking the form of total wave function $\overline{\Psi}(\mathbf{r}_1,\mathbf{r}_2,\ldots,\mathbf{r}_N,t)=\Psi(\mathbf{r}_1,\mathbf{r}_2,\ldots,\mathbf{r}_N)F(t)$ to yield

$$\hat{H}(\mathbf{r}_1,\mathbf{r}_2,\ldots,\mathbf{r}_N)\Psi(\mathbf{r}_1,\mathbf{r}_2,\ldots,\mathbf{r}_N)=E\Psi(\mathbf{r}_1,\mathbf{r}_2,\ldots,\mathbf{r}_N) \tag{2}$$

Here,

$$\hat{H}=\hat{T}_e+\hat{T}_{nuclei}+\hat{V}_{ext}+\hat{U}_{nuclei}+\hat{U}_{ee} \tag{3}$$

where $\hat{T}_e=-\dfrac{\hbar^2}{2m_e}\sum_i \nabla_i^2$ is the kinetic energy operator for electrons with m_e the electron mass;

$\hat{T}_{nuclei}=-\sum_A \dfrac{\hbar^2}{2M_A}\nabla_A^2$ is the kinetic energy operator for nuclei with M_A the mass of the A-th

nucleus; $\hat{V}_{ext}=-\sum_{A,i}\dfrac{Z_A e^2}{4\pi\varepsilon_0|\mathbf{r}_i-\mathbf{R}_A|}$ is the coulomb potential operator for the interaction between

electrons and nuclei with Z_A the charge number of the A-th nucleus, e the absolute value of

electron charge and ε_0 the permittivity of free space; $\hat{U}_{nuclei}=\sum_{A>B}\dfrac{Z_A Z_B e^2}{4\pi\varepsilon_0|\mathbf{R}_A-\mathbf{R}_B|}$ is the coulomb

potential operator for the interaction between nuclei; $\hat{U}_{ee}=\sum_{i>j}\dfrac{e^2}{4\pi\varepsilon_0|\mathbf{r}_i-\mathbf{r}_j|}$ is the coulomb

potential operator for the interaction between electrons; $\mathbf{r}_i$ and $\mathbf{R}_A$ are the position vectors of the i-th electron and the A-th nucleus, respectively; and E is the total energy.

For large molecular system with many electrons and nuclei, equation (2) involves large degrees of freedom. In the potential terms, the coulomb forces of pair interaction between electron-electron and electron-nucleus are accounted, leading to a highly coupled problem.

In the atomic/molecular system, the nuclei are much more massive than the electrons and the electrons move much faster than the nuclei. The Born-Oppenheimer approximation [48] can be used to separate the electron wave function ψ_e from the total wave function Ψ by an assumption that the nuclei are nearly stationary in space with respect to the motion of electrons. Therefore, equation (2) can be simplified as

$$\hat{H}_e\psi_e(\mathbf{r},\mathbf{R})=E_e\psi_e(\mathbf{r},\mathbf{R}) \tag{4}$$

where $\hat{H}_e$ is the electron Hamiltonian operator:

$$\hat{H}_e = \hat{T}_e + \hat{V}_{ext} + \hat{U}_{ee} \tag{5}$$

, and E_e is the total energy of electrons. The total electron wave function ψ_e can be approximated by a set of single electron wave functions, and each of them describes the motion of corresponding electron:

$$\psi_e(\mathbf{r}_1, \mathbf{r}_2, \ldots, \mathbf{r}_N) = \frac{1}{\sqrt{N!}} \begin{vmatrix} \psi_1(\mathbf{r}_1) & \psi_2(\mathbf{r}_1) & \cdots & \psi_N(\mathbf{r}_1) \\ \psi_1(\mathbf{r}_2) & \psi_2(\mathbf{r}_2) & \cdots & \psi_N(\mathbf{r}_2) \\ \vdots & \vdots & \ddots & \vdots \\ \psi_1(\mathbf{r}_N) & \psi_2(\mathbf{r}_N) & \cdots & \psi_N(\mathbf{r}_N) \end{vmatrix} \tag{6}$$

where N is number of electrons.

The pair interaction term $\hat{U}_{ee}$ in electron Hamiltonian operator (5) can be approximated by the interaction between each single electron and an average density field defined as [26]

$$\rho_{avg} = \sum_{i=1}^{N} \rho_i = \sum_{i=1}^{N} |\psi_i|^2 \tag{7}$$

where ψ_i is single electron wave function. Figure 1 shows the electron density of the first four orbitals in Hydrogen atomic structure.
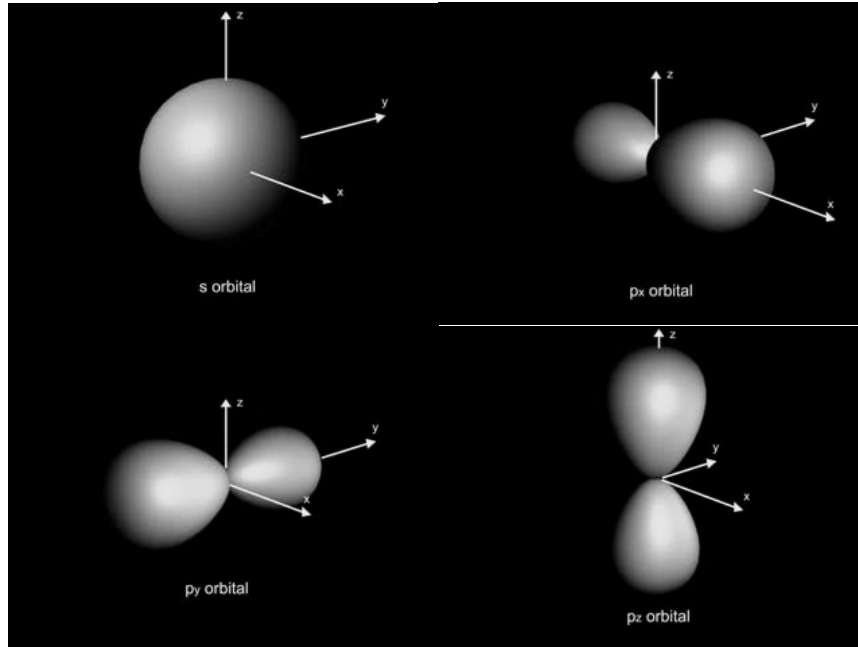

Figure 1.   Electron density distribution of the first four orbitals in Hydrogen atomic structure

Based on the definition of (6), (7) and the energy conservation of the whole system, single electron Schrödinger equation can be constructed in atomic unit (a.u.) where the standard unit is normalized by the mass and charge of electron to yield:

$$\hat{H}_i \psi_i = E_i \psi_i \tag{8}$$

where

$$\hat{H}_i = -\frac{1}{2}\nabla_i^2 - \sum_A \frac{Z_A}{|\mathbf{r}_i - \mathbf{R}_A|} + \hat{g}_i(\mathbf{r})$$

$$\hat{g}_i(\mathbf{r}) = \int \frac{\rho_{avg} - \rho_i}{|\tilde{\mathbf{r}} - \mathbf{r}|} d\tilde{\mathbf{r}} \tag{9}$$

Traditional *ab initio* calculation based on the formulation described above requires computation of wave functions for each electron in the whole quantum system. Alternatively, density functional theory (DFT) [42] that describes the electron motion by electron density instead of wave function results in a system with greatly reduced degrees of freedom. In DFT, the governing equation is obtained by variational principle:

$$\delta\left\{ E(\rho(\mathbf{r})) - \mu\left[\int \rho(\mathbf{r}) d\mathbf{r} - N\right] \right\} = 0 \tag{10}$$

where $E(\rho(\mathbf{r}))$ is total energy expressed by density function $\rho(\mathbf{r})$, μ is a Lagrange multiplier used to impose the constraint on density function $\rho(\mathbf{r})$, and N is the total number of electrons. To express energy by density function in DFT, Kohn-Sham approximation [30] has been introduced by employing the Kohn-Sham wave function ψ_i^{KS} into DFT, and the kinetic energy can be approximated by

$$T(\rho) = \sum_{i=1}^N -\frac{1}{2}\int \tilde{\psi}_i^{KS}(\rho)\nabla^2\psi_i^{KS}(\rho) dr_i \tag{11}$$

where $\psi_i^{KS}(\rho)$ is Kohn-Sham wave function, and $\tilde{\psi}_i^{KS}(\rho)$ is its complex conjugate. Potential operator of DFT can be constructed as:

$$\hat{V}_{eff}(\rho) = \hat{V}_{ext}(\rho) + \hat{U}_{ee}(\rho) + \hat{V}_{xc}(\rho) \tag{12}$$

where

$$\hat{U}_{ee}(\rho) = \int \frac{\rho(\tilde{\mathbf{r}})}{|\tilde{\mathbf{r}} - \mathbf{r}|} d\tilde{\mathbf{r}}, \quad \hat{V}_{ext}(\rho) = \sum_A -\frac{Z_A}{|\mathbf{r} - \mathbf{R}_A|}, \tag{13}$$

and $\hat{V}_{xc}(\rho)$ is a correction term to account for exchange-correlation energy and error introduced in (11). For simple electronic structures, the contribution of $\hat{V}_{xc}(\rho)$ is sufficiently small

compared to other potential functions and is often omitted in numerical calculation [27]. Based on (11) and (12), and following [30], the DFT based Schrödinger equation for $\psi_i^{KS}(\rho)$ can be obtained as

$$\left[-\frac{1}{2}\nabla^2 + \hat{V}_{eff}\left(\rho(\mathbf{r})\right)\right]\psi_i^{KS}\left(\rho(\mathbf{r})\right) = \varepsilon_i \psi_i^{KS}\left(\rho(\mathbf{r})\right) \tag{14}$$

where ε_i is the i-th Kohn-Sham energy corresponding to Kohn-Sham wave function ψ_i^{KS}, and the total energy can be calculated as follows based on ε_i and ρ [30]:

$$E = \sum_{i=1}^{N}\varepsilon_i - \frac{1}{2}\iint \frac{\rho(\tilde{\mathbf{r}})\rho(\mathbf{r})}{|\tilde{\mathbf{r}}-\mathbf{r}|}d\tilde{\mathbf{r}}d\mathbf{r} \tag{15}$$

Both classical Schrödinger equation in (8) and DFT based Schrödinger equation in (14) exhibit highly nonlinear behavior in the region close to the nuclei. The commonly used basis set calculation approximates the wave function by the linear combination of a set of orbital functions $g_k(\mathbf{r})$

$$\psi_i(\mathbf{r}) = \sum_k c_{ki}g_k(\mathbf{r}) \tag{16}$$

In atomic/molecular system, Gaussian type orbital functions (GTOs) and Slater type orbital functions (STOs) have shown to provide an accurate description for electron motion. For example, three-dimensional STOs have the following expressions

$$g_{1s} = \left(\frac{\xi_1^3}{\pi}\right)^{1/2}\exp(-\xi_1 r), \quad g_{2s} = \left(\frac{\xi_2^5}{96\pi}\right)^{1/2}r\exp\left(\frac{-\xi_2 r}{2}\right), \quad g_{2p_x} = \left(\frac{\xi_2^5}{32\pi}\right)^{1/2}x\exp\left(\frac{-\xi_2 r}{2}\right), \quad \dots \tag{17}$$

where $1s, 2s, 2p_x$ are the standard symbols in quantum physics denoting the first principle orbital (spherically symmetric), the first sub-level (spherically symmetric) of the second principle orbital and the second sub-level (x-symmetric) of the second principle orbital, etc., r is the distance measured from the nucleus to the electron, and ξ_i is the scaling parameter representing the size of the atom/molecule. However, these orbital functions are global functions, leading to a full matrix in basis set calculation.

3. Orbital HP-Clouds

3.1. Partition of Unity

Consider an open bounded domain $\Omega \in R^n$, n=1, 2, or 3, with boundary $\partial\Omega$, and let S be a set of N points in $\bar{\Omega} = \Omega \cup \partial\Omega$

7

$$S = \{\mathbf{r}_1, \mathbf{r}_2, \ldots, \mathbf{r}_N\}, \quad \mathbf{r}_I \in \overline{\Omega}, \; I = 1, 2, \ldots, N \tag{18}$$

The set S is used to define a finite open covering $C = \{\omega_I\}_{I=1}^{N}$ of Ω, where $\Omega \subset \cup_{I=1}^{N} \omega_I$. A class of functions $\{\phi_I(\mathbf{r})\}_{I=1}^{N}$ is called a partition of unity subordinated to the open covering C if it possesses the following property:

$$\sum_{I=1}^{N} \phi_I(\mathbf{r}) = 1, \quad \forall \mathbf{r} \in \Omega, \tag{19}$$

and ϕ_I has finite cover ω_I. The partition of unity function can be constructed by

$$\phi_I(\mathbf{r}) = \varphi_I(\mathbf{r}) a(\mathbf{r}) \tag{20}$$

where $\varphi_I(\mathbf{r}) := \varphi(\mathbf{r} - \mathbf{r}_I)$ is a kernel function defined on the finite cover ω_I centered at $\mathbf{r}_I$, and $a(\mathbf{r})$ is a function to be thought to meet partition of unity condition. By substituting (20) into (19), one has

$$\left(\sum_{J=1}^{N} \varphi_J(\mathbf{r}) \right) a(\mathbf{r}) = 1 \tag{21}$$

By obtaining $a(\mathbf{r}) = 1 / \sum_{J=1}^{N} \varphi_J(\mathbf{r})$, the function in (20) yields:

$$\phi_I(\mathbf{r}) = \frac{\varphi_I(\mathbf{r})}{\sum_{J=1}^{N} \varphi_J(\mathbf{r})} \tag{22}$$

The partition of unity function in Eq. (22) is the Shepard function.

3.2 Intrinsic and Extrinsic Enrichments
To embed fundamental characteristics of the quantum system into the numerical approximation function, an intrinsic enrichment with orbital functions is introduced. For demonstration purpose, the first STO function $e^{-\xi r}$ in (17) is used herein. Other orbital functions can also be considered. We start with the correction of kernel function as

$$\phi_I(\mathbf{r}) = \varphi_I(\mathbf{r}) \left[a_0(\mathbf{r}) + e^{-\xi r_I} a_1(\mathbf{r}) \right], \quad r_I = \|\mathbf{r}_I\| \tag{23}$$

Note that here the coefficients $a_0(\mathbf{r})$ and $a_1(\mathbf{r})$ are to be obtained by reproducibility of 1 and $e^{-\xi r}$ as

$$\begin{cases} \sum_{I=1}^{N} \phi_I(\mathbf{r}) = 1 \\ \sum_{I=1}^{N} \phi_I(\mathbf{r}) e^{-\xi r_I} = e^{-\xi r} \end{cases}$$

(24)

Thus we have the following two equations:

$$\left\{ \sum_{I}^{N} \varphi_I(\mathbf{r}) \begin{bmatrix} 1 \\ e^{-\xi r_I} \end{bmatrix} \begin{bmatrix} 1 & e^{-\xi r_I} \end{bmatrix} \right\} \begin{bmatrix} a_0(\mathbf{r}) \\ a_1(\mathbf{r}) \end{bmatrix} = \begin{bmatrix} 1 \\ e^{-\xi r} \end{bmatrix}$$

(25)

or

$$\mathbf{A}(\mathbf{r})\mathbf{a}(\mathbf{r}) = \mathbf{b}(\mathbf{r})$$

(26)

where

$$\mathbf{A}(\mathbf{r}) = \sum_{I}^{N} \varphi_I(\mathbf{r})\mathbf{b}(\mathbf{r}_I)\mathbf{b}^T(\mathbf{r}_I), \quad \mathbf{b}^T(\mathbf{r}) = \begin{bmatrix} 1 & e^{-\xi r} \end{bmatrix}, \quad \mathbf{a}^T(\mathbf{r}) = \begin{bmatrix} a_0(\mathbf{r}) & a_1(\mathbf{r}) \end{bmatrix}$$

(27)

The resulting intrinsically enriched function is

$$\phi_I(\mathbf{r}) = \mathbf{b}^T(\mathbf{r}_I)\mathbf{A}^{-1}(\mathbf{r})\mathbf{b}(\mathbf{r})\varphi_I(\mathbf{r})$$

(28)

The global approximation of the wave function Ψ, denoted as Ψ^h, is constructed by using the set of partition of unity functions $\{\phi_I(\mathbf{r})\}_{I=1}^{N}$ and monomial extrinsic enrichment functions as

$$\begin{aligned} \Psi^h(\mathbf{r}) &= \sum_{I=1}^{N} \phi_I(\mathbf{r}) \left[\sum_{i=1}^{n} P_i(\mathbf{r} - \mathbf{r}_I)\alpha_I^i \right] \\ &= \sum_{I=1}^{N} \sum_{i=1}^{n} \phi_I(\mathbf{r}) P_i(\mathbf{r} - \mathbf{r}_I)\alpha_I^i \\ &= \sum_{I=1}^{N} \sum_{i=1}^{n} \Phi_I^i(\mathbf{r})\alpha_I^i \\ &= \mathbf{\Phi}^T \boldsymbol{\alpha} \end{aligned}$$

(29)

where $\{P_i(\mathbf{r} - \mathbf{r}_I)\}_{i=1}^{n}$ is a set of shifted monomial functions, $\Phi_I^i(\mathbf{r}) = \phi_I(\mathbf{r})P_i(\mathbf{r} - \mathbf{r}_I)$, and

$$\begin{aligned} \mathbf{\Phi}^T &= \begin{bmatrix} \mathbf{\Phi}_1^T & \mathbf{\Phi}_2^T & \cdots & \mathbf{\Phi}_N^T \end{bmatrix}, \quad \mathbf{\Phi}_I^T = \begin{bmatrix} \Phi_I^1 & \Phi_I^2 & \cdots & \Phi_I^n \end{bmatrix}, \\ \boldsymbol{\alpha}^T &= \begin{bmatrix} \boldsymbol{\alpha}_1^T & \boldsymbol{\alpha}_2^T & \cdots & \boldsymbol{\alpha}_N^T \end{bmatrix}, \quad \boldsymbol{\alpha}_I^T = \begin{bmatrix} \alpha_I^1 & \alpha_I^2 & \cdots & \alpha_I^n \end{bmatrix} \end{aligned}$$

(30)

Note that this orbital HP-Cloud approximation has locality: $\mathrm{supp}(\Phi_I^i) = \mathrm{supp}(\phi_I) = \omega_I$.

4. Galerkin Approximation of Schrödinger Equation

4.1 Discretization
In atomic/molecular systems, the static Schrödinger equation can be expressed by

$$\left[-\frac{\nabla^2}{2} + \hat{V} \right] \Psi(\mathbf{r}) = \varepsilon \Psi(\mathbf{r}) \tag{31}$$

subjected to the approximated boundary condition:

$$\Psi = 0 \quad \text{on} \quad \partial\Omega \tag{32}$$

where in the classical Schrödinger equation, $\hat{V}$ is the coulomb potential function, Ψ is the electron wave function, and ε is the total energy. While for DFT based Schrödinger equation, $\hat{V}$ is the effective potential, Ψ is the Kohn-Sham wave function, and ε is the Kohn-Sham energy. The boundary $\partial\Omega$ is the cut-off boundary and Eq. (32) is an approximation of $\lim\limits_{\|\mathbf{r}\|\to\infty} \Psi(\mathbf{r}) = 0$. For example, in a Hydrogen structure, the wave function $\Psi(\mathbf{r}) < 10^{-3}$ when $\|\mathbf{r}\| > 5$ a.u. (atomic unit) for the first energy level, $\|\mathbf{r}\| > 15$ a.u. for the second energy level, and $\|\mathbf{r}\| > 20$ a.u. for the third energy level. For other multi-particle systems considered in this work, the electron density is more concentrated at the nucleus, leading to a faster decay in the wave function. The cut-off boundary of $\|\mathbf{r}\| = 5$ a.u. for the first energy level has been used by White et al. [53] for FEM model of Hydrogen atom.

The Galerkin approximation of this problem is to find $\Psi^h \in H_0^1$, $\forall \Lambda^h \in H_0^1$, such that

$$\int_\Omega \left[\frac{\nabla \Lambda^h(\mathbf{r}) \cdot \nabla \Psi^h(\mathbf{r})}{2} + \Lambda^h(\mathbf{r})\Psi^h(\mathbf{r})\hat{V}(\mathbf{r}) \right] d\Omega = \varepsilon^h \int_\Omega \left[\Lambda^h(\mathbf{r})\Psi^h(\mathbf{r}) \right] d\Omega \tag{33}$$

Note that when bilinear basis functions are included in the extrinsic enrichment, the resulting shape function with rectangular cover coincides with the closest uniformly distributed neighboring point yields a finite element shape function between points. We consider using this approach for the discrete points at the most outside layer of the numerical domain so that the approximation of Ψ and Λ can be made kinematically admissible to the homogeneous boundary conditions on $\partial\Omega$, and thus fulfill the approximation space H_0^1 in the weak form.

The test and trial functions are approximated by the orbital HP-Cloud approximation (29)

$$\begin{aligned} \Psi^h(\mathbf{r}) &= \Phi^T(\mathbf{r})\alpha \\ \Lambda^h(\mathbf{r}) &= \Phi^T(\mathbf{r})\beta \end{aligned} \tag{34}$$

The resulting discrete equation of (33) reads:

$$\mathbf{K}\alpha = \varepsilon^h \mathbf{S}\alpha \tag{35}$$

where

$$\mathbf{K}_{IJ} = \int_\Omega \left[\frac{\left(\nabla\Phi_I^T\right)^T \nabla\Phi_J^T}{2} + \Phi_I\Phi_J^T\hat{V}(\mathbf{r}) \right] d\Omega, \quad \nabla\Phi_J^T = \begin{bmatrix} \dfrac{\partial\Phi_J^T}{\partial r_1} \\[2mm] \dfrac{\partial\Phi_J^T}{\partial r_2} \\[2mm] \dfrac{\partial\Phi_J^T}{\partial r_3} \end{bmatrix} \tag{36}$$

$$\mathbf{S}_{IJ} = \int_\Omega \left(\Phi_I\Phi_J^T \right) d\Omega \tag{37}$$

In the single-electron system, the classical Schrödinger equation is solved, and potential function $\hat{V}$ is independent to the electron density. Thus, (35) is a linear eigenvalue problem and can be solved with the standard method. For multi-electron systems, DFT based Schrödinger equation is employed to deal with the interaction between all electrons. In this case $\hat{V}$ is a function of the electron density, and (35) needs to be solved iteratively.

4.2 Stabilized Conforming Nodal Integration (SCNI)
Domain integration of weak form poses considerable complexity in Galerkin meshfree method. Employment of Gauss quadrature rules yields integration error when background grids do not coincide with the covers of shape functions. Direct nodal integration, on the other hand, results in rank deficiency. Both methods do not pass linear patch test for non uniform point distribution. A stabilization conforming nodal integration (SCNI) [17] has been introduced to satisfy linear patch test and to remedy rank deficiency of direct nodal integration. For demonstration, consider here a Poisson problem as the model problem:

$$\nabla^2 u + Q = 0 \ \ \text{in} \ \ \Omega \tag{38}$$

with homogeneous Dirichlet boundary. The corresponding Galerkin approximation is to find $u^h \in H_0^1$, $\forall v^h \in H_0^1$,

$$\int_\Omega \nabla v^h \cdot \nabla u^h d\Omega = \int_\Omega v^h Q d\Omega \tag{39}$$

Performing nodal integration of the above equations results in

$$\sum_{L=1}^N \nabla v^h(\mathbf{r}_L) \cdot \nabla u^h(\mathbf{r}_L) w_L = \sum_{L=1}^N v^h(\mathbf{r}_L) Q(\mathbf{r}_L) w_L \tag{40}$$

11

where w_L is the weight associated with point L. Applying HP-Cloud approximation of the test and trial functions in (40), leads to a rank deficient discrete system and fails in passing a linear patch test. Consider a SCNI approach [17], where a smoothed gradient operator at nodal point $\mathbf{r}_L$ is introduced as

$$\bar{\nabla}u^h\left(\mathbf{r}_L\right)=\frac{1}{w_L}\int_{\Omega_L}\nabla u^h d\Omega=\frac{1}{w_L}\int_{\partial\Omega_L}u^h\mathbf{n}d\Gamma, \quad w_L=\int_{\Omega_L}d\Omega \tag{41}$$

Here Ω_L is the nodal representative domain, which can be obtained from triangulation or Voronoi cell of a set of discrete points as shown in Figure 2. Note that a divergence theorem has been used in (41) to pass the linear patch test when the weak form is integrated by nodal integration [17]. Introducing approximation of u, $u^h=\sum_{I=1}^{N}\Phi_I^T\mathbf{d}_I$, into (41), we have

$$\bar{\nabla}u^h\left(\mathbf{r}_L\right)=\sum_{I=1}^{N}\bar{\mathbf{B}}_I\left(\mathbf{r}_L\right)\mathbf{d}_I \tag{42}$$

where

$$\bar{\mathbf{B}}_I\left(\mathbf{r}_L\right)=\frac{1}{w_L}\int_{\partial\Omega_L}\mathbf{n}\Phi_I^T d\Gamma \tag{43}$$
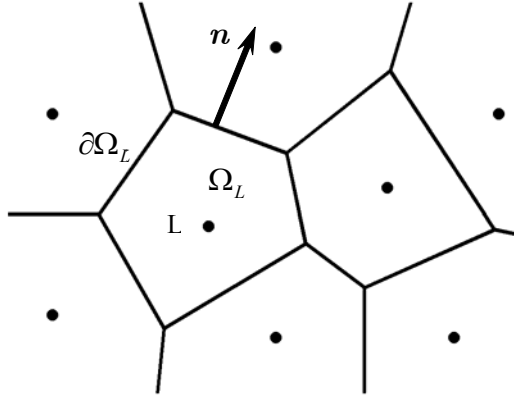

Figure 2. Nodal representative domain

Introducing the smoothed gradient of (42) into weak form yields the following discrete equation:

$$\sum_{L=1}^{N}\bar{\nabla}v^h\left(\mathbf{r}_L\right)\cdot\bar{\nabla}u^h\left(\mathbf{r}_L\right)w_L=\sum_{L=1}^{N}v^h\left(\mathbf{r}_L\right)Q\left(\mathbf{r}_L\right)w_L \tag{44}$$

and hence

$$\mathbf{Kd}=\mathbf{f} \tag{45}$$

where

$$\mathbf{K}_{IJ} = \sum_{L=1}^{N} \overline{\mathbf{B}}_I^T (\mathbf{r}_L) \overline{\mathbf{B}}_J (\mathbf{r}_L) w_L, \quad w_L = \int_{\Omega_L} d\Omega \tag{46}$$

$$\mathbf{f}_I = \sum_{L=1}^{N} \mathbf{\Phi}_I (\mathbf{r}_L) Q(\mathbf{r}_L) w_L \tag{47}$$

4.3 Higher Order SCNI (HSCNI)

Although the discrete equation (45) passes a linear patch test, the SCNI only offers lower order accuracy and is insufficient when higher order basis functions are employed, such as the orbital HP-Cloud approximation introduced in this work. To achieve a higher order accuracy in domain integration of weak form of Schrödinger equation with orbital HP-Cloud approximation, we introduce a correction to SCNI. First, consider the following identity associated with Laplace operator:

$$\int_{\Omega_L} \nabla v^h(\mathbf{r}) \cdot \nabla u^h(\mathbf{r}) d\Omega = \overline{\nabla} v^h(\mathbf{r}_L) \cdot \overline{\nabla} u^h(\mathbf{r}_L) w_L + \int_{\Omega_L} \left(\nabla v^h(\mathbf{r}) - \overline{\nabla} v^h(\mathbf{r}_L) \right) \cdot \left(\nabla u^h(\mathbf{r}) - \overline{\nabla} u^h(\mathbf{r}_L) \right) d\Omega \tag{48}$$

To show this identity, examine the right hand side of this equation:

$$\overline{\nabla} v^h(\mathbf{r}_L) \cdot \overline{\nabla} u^h(\mathbf{r}_L) w_L + \int_{\Omega_L} \left(\nabla v^h(\mathbf{r}) - \overline{\nabla} v^h(\mathbf{r}_L) \right) \cdot \left(\nabla u^h(\mathbf{r}) - \overline{\nabla} u^h(\mathbf{r}_L) \right) d\Omega$$

$$= \overline{\nabla} v^h(\mathbf{r}_L) \cdot \overline{\nabla} u^h(\mathbf{r}_L) w_L + \int_{\Omega_L} \nabla v^h(\mathbf{r}) \cdot \nabla u^h(\mathbf{r}) d\Omega - \int_{\Omega_L} \nabla v^h(\mathbf{r}) d\Omega \cdot \overline{\nabla} u^h(\mathbf{r}_L) \tag{49}$$

$$- \overline{\nabla} v^h(\mathbf{r}_L) \cdot \int_{\Omega_L} \nabla u^h(\mathbf{r}) d\Omega + \overline{\nabla} v^h(\mathbf{r}_L) \cdot \overline{\nabla} u^h(\mathbf{r}_L) w_L$$

Recall the smoothed gradient, $\int_{\Omega_L} \nabla u^h d\Omega = \overline{\nabla} u^h(\mathbf{r}_L) w_L$, (49) can be reduced to $\int_{\Omega_L} \nabla v^h(\mathbf{r}) \cdot \nabla u^h(\mathbf{r}) d\Omega$, and this proves (48). By summing up all nodal points in (48) we have

$$\int_{\Omega} \nabla v^h(\mathbf{r}) \cdot \nabla u^h(\mathbf{r}) d\Omega$$

$$= \sum_{L=1}^{N} \overline{\nabla} v^h(\mathbf{r}_L) \cdot \overline{\nabla} u^h(\mathbf{r}_L) w_L + \underbrace{\sum_{L=1}^{N} \int_{\Omega_L} \left(\nabla v^h(\mathbf{r}) - \overline{\nabla} v^h(\mathbf{r}_L) \right) \cdot \left(\nabla u^h(\mathbf{r}) - \overline{\nabla} u^h(\mathbf{r}_L) \right) d\Omega}_{correction\ term} \tag{50}$$

Now one could use n-th order Gauss integration on left or right side of (50) and expect to get the same results, provided that $\overline{\nabla} u^h(\mathbf{r}_L)$ (and $\overline{\nabla} v^h(\mathbf{r}_L)$) is integrated using the same Gauss rule. If u is approximated by polynomial functions, we still don't recover 1st order patch test using standard Gauss integration in (50) as is well known. However if we compute $\overline{\nabla} u^h(\mathbf{r}_L)$ (and

$\bar{\nabla} v^h (\mathbf{r}_L))$ numerically by its divergence counterpart using (41), since in linear patch test u is linear, $\nabla u(\mathbf{r}) - \bar{\nabla} u(\mathbf{r}_L) = 0$, and (50) reduces to standard SCNI and thus passes linear patch test, regardless of the order of quadrature rule used in the boundary integral of $\bar{\nabla} u^h (\mathbf{r}_L)$ according to Chen et al. [17].

To achieve higher order accuracy and to pass linear patch test, in (39) $\int_\Omega \nabla v^h(\mathbf{r}) \cdot \nabla u^h(\mathbf{r}) d\Omega$ is computed by (50) where $\sum_{L=1}^{N} \int_{\Omega_L} (\nabla v^h(\mathbf{r}) - \bar{\nabla} v^h(\mathbf{r}_L)) \cdot (\nabla u^h(\mathbf{r}) - \bar{\nabla} u^h(\mathbf{r}_L)) d\Omega$ is integrated using *n*-th order Gauss integration and $\bar{\nabla} u^h(\mathbf{r}_L)$ and $\bar{\nabla} v^h(\mathbf{r}_L)$ are computed by (41) using boundary integration consistent with Gauss quadrature rule used in domain integration as shown in Figure 3. For irregular shape nodal domain, triangular quadrature rules can be used.

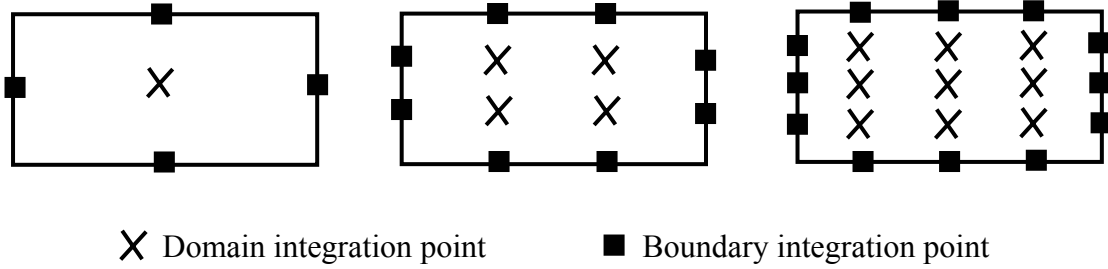✗ Domain integration point   ■ Boundary integration point

Figure 3.   Consistent domain and boundary integration points in HSCNI

The Schrödinger equation in (33) is now integrated according to HSCNI in (50) to yield

$$\frac{1}{2}\sum_{L=1}^{N} \bar{\nabla} \Lambda^h(\mathbf{r}_L) \cdot \bar{\nabla} \Psi^h(\mathbf{r}_L) w_L + \frac{1}{2}\sum_{L=1}^{N} \int_{\Omega_L} (\nabla \Lambda^h(\mathbf{r}) - \bar{\nabla} \Lambda^h(\mathbf{r}_L)) \cdot (\nabla \Psi^h(\mathbf{r}) - \bar{\nabla} \Psi^h(\mathbf{r}_L)) d\Omega$$
$$+ \sum_{L=1}^{N} \int_{\Omega_L} \Lambda^h(\mathbf{r}) \hat{V} \Psi^h(\mathbf{r}) d\Omega = \varepsilon \sum_{L=1}^{N} \int_{\Omega_L} \Lambda^h(\mathbf{r}) \Psi^h(\mathbf{r}) d\Omega \tag{51}$$

By introducing orbital HP-Cloud approximation to Ψ and Λ in (51), the discrete equation is obtain similar to (35)-(37), except that $\mathbf{K}_{IJ}$ is replaced by

$$\mathbf{K}_{IJ} = \sum_{L=1}^{N} \{ \frac{1}{2} (\bar{\nabla} \Phi_I^T(\mathbf{r}_L))^T \bar{\nabla} \Phi_J^T(\mathbf{r}_L) w_L$$
$$+ \int_{\Omega_L} \left[\frac{1}{2} (\nabla \Phi_I^T - \bar{\nabla} \Phi_I^T(\mathbf{r}_L))^T (\nabla \Phi_J^T - \bar{\nabla} \Phi_J^T(\mathbf{r}_L)) + \Phi_I \Phi_J^T \hat{V}(\mathbf{r}) \right] d\Omega \} \tag{52}$$

where

$$\bar{\nabla}\Phi_I(\mathbf{r}_L) = \frac{1}{w_L}\int_{\partial\Omega_L}\mathbf{n}\Phi_I d\Gamma, \quad w_L = \int_{\Omega_L} d\Omega \tag{53}$$

4.4 Numerical Test of HSCNI

4.4.1 Poisson Problem

With HSCNI, higher order accuracy and optimal convergence rate can be achieved by increasing the order of Gaussian integration for the correction term in (50) and force vector, and the method passes linear patch test. In this example we consider a 2-dimensional Poisson equation:

$$\begin{cases} \nabla^2 u(x,y) = -2\pi^2 \sin(\pi x)\sin(\pi y) & (x,y) \in (0,1)\times(0,1) \equiv \Omega \\ \qquad u = 0 & \partial\Omega \end{cases} \tag{54}$$

The analytical solution of this problem is $\sin(\pi x)\sin(\pi y)$. We employed HP-Cloud approximation with complete linear and quadratic monomial bases in the intrinsic enrichment. Third order Gauss quadrature rule is employed in HSCNI. The convergence rate of the L2 error norm in Figure 5 shows that a better accuracy and convergence rate of HSCNI than those of SCNI for both analyses using linear and quadratic polynomial bases, especially when higher order basis functions are employed.
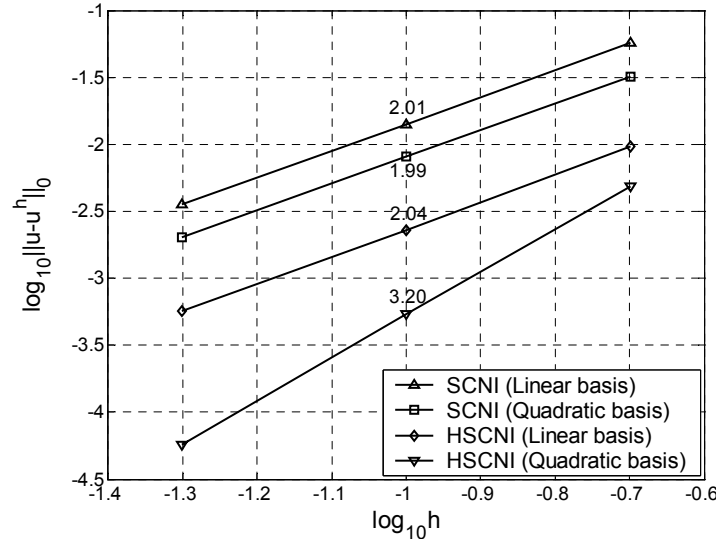

Figure 5.   Convergence rate of L2 error norm in 2D Poisson equation

4.4.2 Differential Equation with Schrödinger Operator

In this example we investigate appropriate order of Gauss quadrature in HSCNI for solving Schrödinger equation. For this purpose, we consider the following differential equation:

$$\begin{cases} -\nabla^2 u(x,y) + (1 - 2\pi^2) u(x,y) = -2\pi e^x \cos(\pi x) \sin(\pi y) & \Omega \equiv (0,1) \otimes (0,1) \\ \quad u(x,y) = 0 & (x,y) \in \partial\Omega \end{cases} \tag{55}$$

This problem mimics the differential operator of the Schrödinger equation. The solution of this problem is $e^x \sin(\pi x) \sin(\pi y)$. We purposely introduce constant function and $e^x \sin(\pi x) \sin(\pi y)$ as the basis functions in the intrinsic enrichment so that the solution error is entirely due to domain integration of weak form. HSCNI is used in the stiffness matrix associated with the Laplace operator, and standard Gauss integration with the same order of quadrature rule in HSCNI is employed for the matrices associated with other terms in the differential equation. Figure 6 shows convergence properties of numerical solution using different quadrature orders in HSCNI.
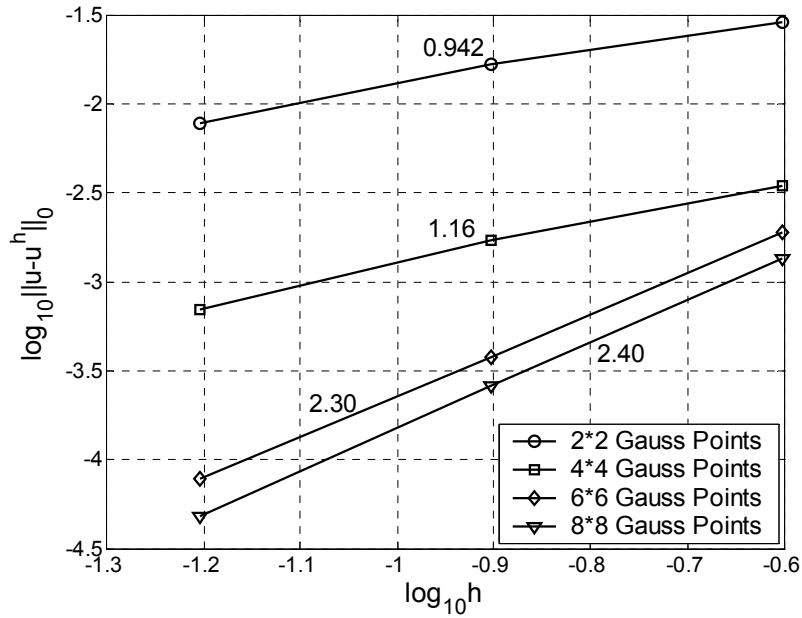

Figure 6.   Convergence rate of L2 error norm in Differential Equation with Schrödinger Operator

5. Numerical Results

The proposed orbital HP-Clouds method is tested in three quantum systems:

(1) Hydrogen atom: one electron and one nucleus with charge +1: The nucleus is located at the center point (Figure 7 (a)).
(2) Hydrogen molecular ion: one electron and two nuclei each with charge +1: Two nuclei are located along x-axis with distance 2 a.u. (Figure 7 (b)).
(3) Hydrogen molecule: two electrons with two nuclei each with charge +1: Two nuclei are located along x-axis with distance 1.4 a.u. (Figure 7 (c)).

16

For a Hydrogen atom structure, $\Psi(\mathbf{r}) < 10^{-3}$ as $\|\mathbf{r}\| > 5$ a.u. for the first energy level, thus we define a computational domain with 10 a.u. in each side of cube as shown in Figure 7 for all three cases in first energy level calculation. Note that for the other two multi-electron/nucleus systems (2) and (3), the electron densities are more concentrated at the nucleus, yielding a faster decay in the wave function compared to the Hydrogen atom structure. Hence the selected computational domain 10 a.u. for system (1) is also used for systems (2) and (3). The value of wave function on the boundary of the cubic domain is assumed to be zero. For calculation of solution on higher energy levels, a larger computational domain is required as discussed in the numerical examples.

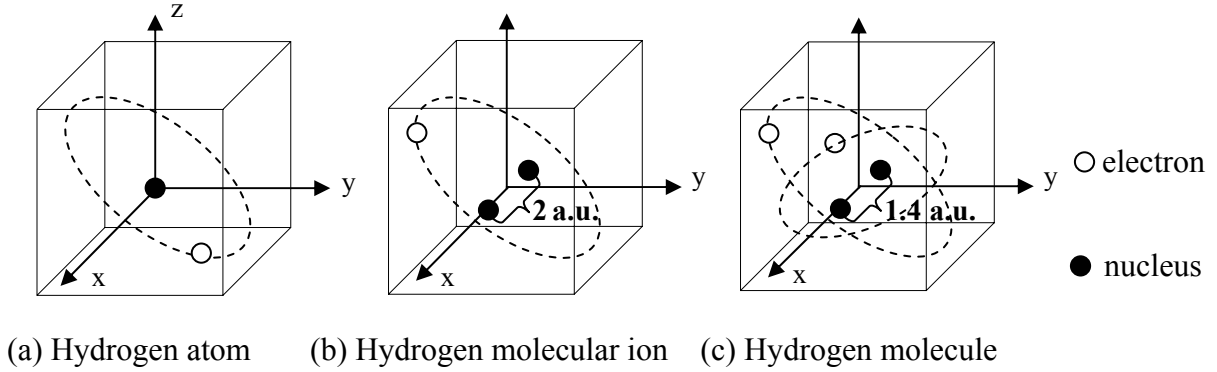(a) Hydrogen atom   (b) Hydrogen molecular ion   (c) Hydrogen molecule

Figure 7.   Three quantum systems and computational domain

For easy discussion, we rewrite the proposed orbital HP-Cloud (OHPC) approximation of wave function as follows:

$$\Psi^h(\mathbf{r}) = \sum_{I=1}^{N} \phi_I(\mathbf{r})\mathbf{h}_I^{ex^T}(\mathbf{r})\boldsymbol{\alpha}_I \tag{56}$$

$$\phi_I(\mathbf{r}) = \varphi_I(\mathbf{r})\mathbf{h}_I^{in^T}(\mathbf{r})\mathbf{a} \tag{57}$$

where $\mathbf{h}_I^{in}$ and $\mathbf{h}_I^{ex}$ are the vectors of intrinsic and extrinsic basis functions, respectively, and $\mathbf{a}$ and $\boldsymbol{\alpha}_I$ are the corresponding coefficient vectors. Note that the intrinsic coefficient vector $\mathbf{a}$ is condensed by imposing reproducing conditions and the global discrete equations only involve $\boldsymbol{\alpha}_I$ as unknowns. In this study, we use cubic B-spline function as the kernel function φ_I to construct the partition of unity. We employ HSCNI for integration of stiffness matrix associated with the Laplace operator, and standard Gauss integration with the same order of quadrature rule in HSCNI is employed for integrating the matrices associated with other terms in the Schrödinger equation. The solutions obtained from the proposed OHPC will be compared with those obtained from 3rd order p-adaptive FEM [53] and FEM approximation enriched with Gaussian function (Gaussian-FEM) [55] in the following study. Note that Gaussian-FEM is a global approximation and thus yields a full matrix in its discrete equation.

For quantum systems (1) and (2), only one electron exists, and thus the standard Schrödinger equation (8) can be used, where the potential function is independent of the electron density. Whereas quantum system (3) contains 2 electrons, and thus Kohn-Sham Schrödinger equation (14) based on the density function theory is employed. The effective potential function is dependent on the electron density and Newton iteration is used in this case.

(1). Hydrogen atom

Since Hydrogen atom is spherical symmetric, the total electron wave function can be expressed by a product of two functions: radial wave function $R(r)$ and spherical harmonic function $Y(\theta,\phi)$. The equation of radial wave function $R(r)$ can be expressed below [13] and will be solved by various numerical methods for comparison:

$$\left[-\frac{1}{2}\frac{1}{r^2}\frac{d}{dr}\left(r^2 \frac{d}{dr} \right) + \frac{l(l+1)}{2r^2} + V(r) \right] R(r) = ER(r) \tag{58}$$

where l is orbital angular quantum number. In this study, we only consider $l = 0$ (principal value) of each energy level. Define a new variable $\bar{R}(r) = rR(r)$, Eq. (58) is reduced to

$$\frac{d^2 \bar{R}(r)}{dr^2} + 2\left[E - V(r) \right] \bar{R}(r) = 0 \tag{59}$$

The one-dimensional characteristic functions $g_i(r)$ of $\bar{R}(r)$ for the first three energy levels are:

$$g_1(r) = re^{-r},\ g_2(r) = re^{-r/2}\left(1 - r/2\right),\ g_3(r) = re^{-r/3}\left(1 - 2r/3 + 2r^2/27\right) \tag{60}$$

As discussed earlier, the cut-off boundary $\|r\| = 10$ a.u. (atomic unit) is used as the numerical domain for the first energy level, whereas $\|r\| = 20$ a.u. is employed for the 2nd and 3rd energy level calculations. Three energy levels obtained using HP-Cloud approximations with first order polynomial intrinsic enrichment (HPC1), second order polynomial intrinsic enrichment (HPC2), and orbital intrinsic enrichment (OHPC) are compared in Table 1. HSCNI with 4th order quadrature rule is employed in all cases. The numerical solution clear shows that OHPC is most effective. Figure 8 compares the predicted solutions $r^2 R^2(r)$ of the first three energy levels using various intrinsic enrichments.

Next, for comparison with 3-dimensional finite element solution of the first energy level [53], a full 3-dimensional Schrödinger equation (8) is solved using OHPC with the following enrichments:

$$\mathbf{h}_I^{in} = \left[1, e^{-\xi r} \right], \quad \mathbf{h}_I^{ex} = \left[1 \right] \tag{61}$$

where $\xi = 1$ for Hydrogen atom. HSCNI with 4th order quadrature rule is employed. The error in the first energy level of this quantum system is compared, where the exact solution of the first

energy level is $E = -0.5$ a.u.. In Figure 9, the orbital HP-Cloud solution is compared to the solution obtained from the 3rd order p-adaptive finite element method [53], where the 3rd order, 2nd order, and 1st order FEM approximation is used in the region $\|r\| \leq 2$ a.u., 2 a.u. $\leq \|r\| \leq 4$ a.u., and $\|r\| \geq 4$ a.u., respectively. Note that since e^{-r} is the 3-dimensional characteristic function of the Hydrogen atom, the numerical error of this problem using HP-Cloud approximation is due to domain integration.

Table 1   Comparison of numerical error of the first three energy levels using one-dimensional HP-Cloud with different intrinsic enrichment functions

Approximation methods	No. of nodes	Error of the first energy level	Error of the second energy level	Error of the third energy level
HPC1: HPC with first order polynomial intrinsic enrichment	41	13.2%	8.23%	5.82%
$\mathbf{h}_I^{in} = \left[1, \dfrac{x_I - x_{II}}{c_I} \right], \mathbf{h}_I^{ex} = [1]$	81	3.71%	2.22%	1.51%
HPC2: HPC with second order polynomial intrinsic enrichment	41	3.68%	1.74%	1.14%
$\mathbf{h}_I^{in} = \left[1, \dfrac{x_I - x_{II}}{c_I}, \left(\dfrac{x_I - x_{II}}{c_I} \right)^2 \right], \mathbf{h}_I^{ex} = [1]$	81	0.331%	0.192%	0.0864%
OHPC: HPC with orbital intrinsic enrichment $\mathbf{h}_I^{in} = \left[1, g_i(r) \right], \mathbf{h}_I^{ex} = [1]$ $g_i(r)$ is chosen from (60) for i-th energy level	21	0.00%	0.162%	0.0102%

(a) 1st energy level   (b) 2nd energy level
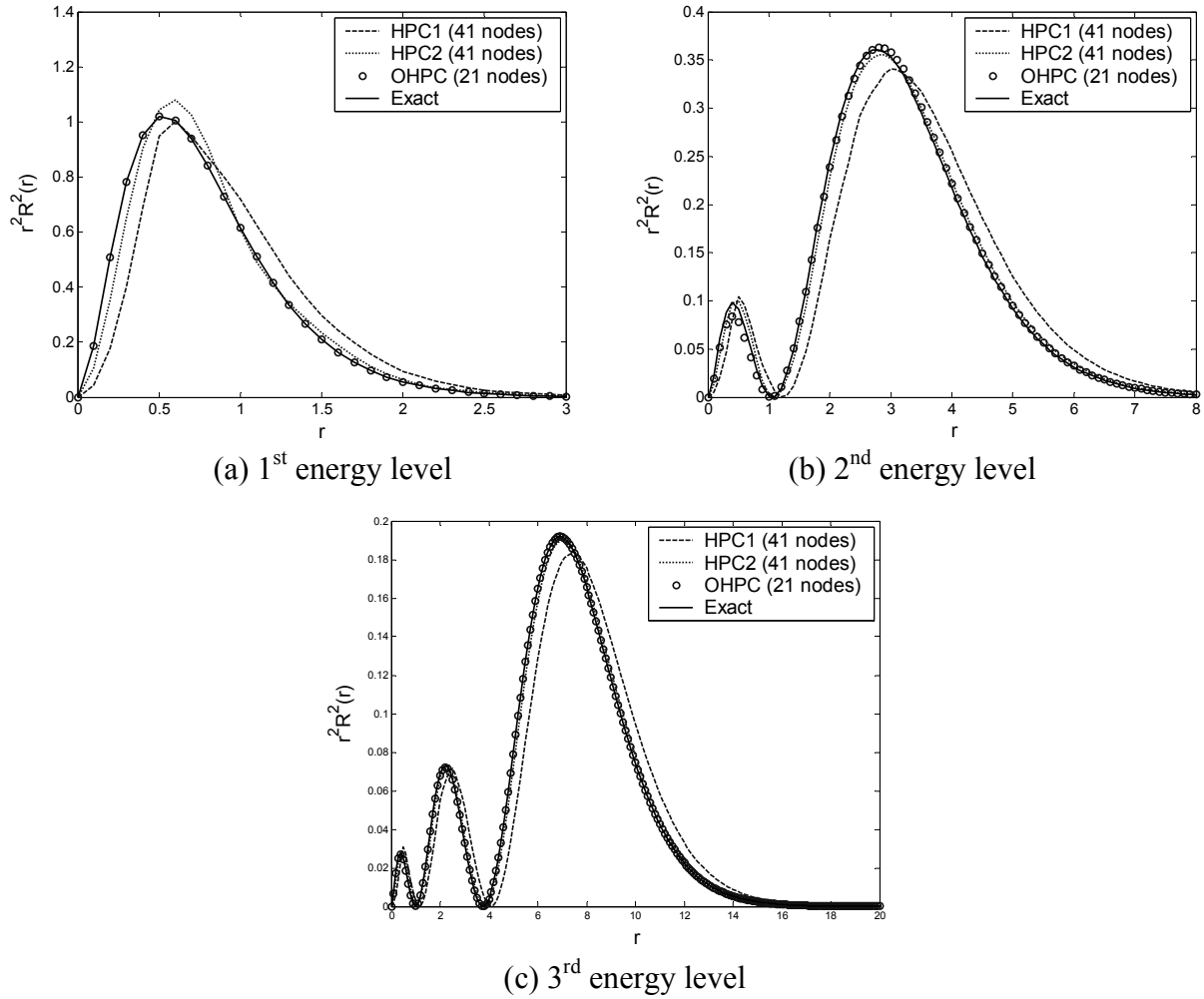
(c) 3rd energy level

Figure 8.   Predicted radial distribution functions $r^2 R^2(r)$ of the first three energy levels

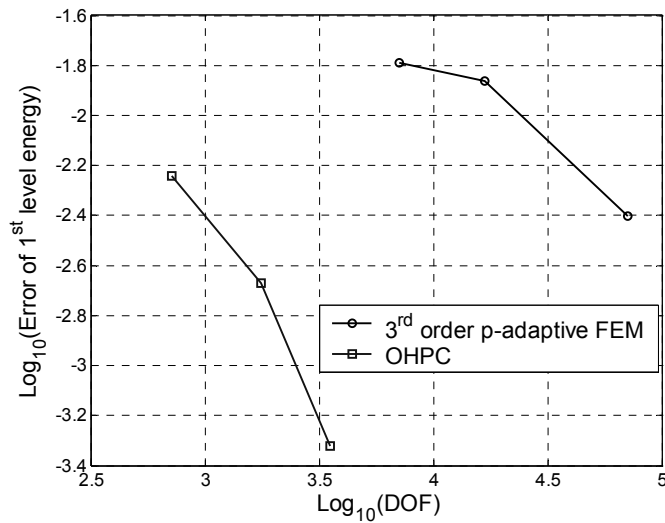

Figure 9.   Numerical error of the first level energy of Hydrogen atom predicted by the 3rd order p-adaptive FEM and OHPC

(2). Hydrogen molecular ion

Since this quantum system (Figure 7 (b)) contains 2 nuclei, we consider the following OHPC approximation:

$$\mathbf{h}_I^{in} = \left[1, e^{-r_1}, e^{-r_2} \right], \quad \mathbf{h}_I^{ex} = \left[1, \frac{x_1 - x_{1I}}{c_1}, \frac{x_2 - x_{2I}}{c_2}, \frac{x_3 - x_{3I}}{c_3} \right] \tag{62}$$

where c_i is the dimension of the cover of kernel function in the i-th direction, and $r_1 = \| \mathbf{r} - \mathbf{R}_1 \|$ and $r_2 = \| \mathbf{r} - \mathbf{R}_2 \|$ are distance measured from the evaluation point to the locations of the 2 nuclei, $\mathbf{R}_1$ and $\mathbf{R}_2$, respectively. In this problem, the orbital bases for Hydrogen atom are only approximations, and linear monomial functions are used as an extrinsic enrichment of OHPC.

We first use the coarsest discretization ($9 \times 9 \times 9$ nodes) to identify the proper order of quadrature in HSCNI for this problem. To capture the very high order behavior in the wave function near nucleus, 2nd, 4th and 8th orders of Gaussian quadrature rule for a small region with dimension of 6 a.u. in each direction, and 2nd order Gauss quadrature rule for the rest of the domain are used. Table 2 lists the results of the first energy level. The reference solution of the first level energy of this quantum system is -1.1026 a.u. [53].

Table 2.   Numerical error of the first level energy for Hydrogen molecule ion

2nd order	4th order	8th order
6.2%	2.0%	1.3%

Based on the results in Table 2, HSCNI with 8th order Gauss quadrature rule is employed in a small region with dimension of 6 a.u. in each direction, and 2nd order Gauss quadrature rule is used for the rest of the domain. The results of the first level energy obtained from OHPC with HSCNI and the 3rd order p-adaptive FEM are compared in Figure 10. Better solution accuracy is obtained by using the proposed OHPC method. Figure 11 displays the electron density distribution $\rho = \Psi^2$ of this Hydrogen molecular ion obtained by the proposed OHPC method.
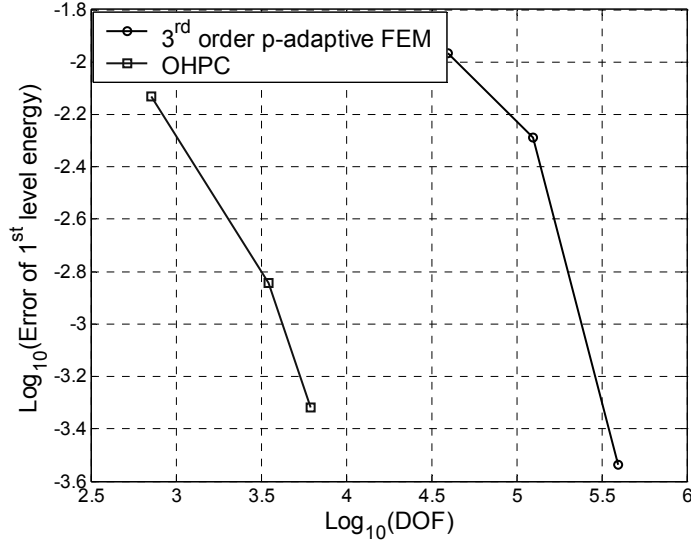
Figure 10.   Numerical error of the first level energy of Hydrogen molecular ion predicted by the 3rd order p-adaptive FEM and OHPC

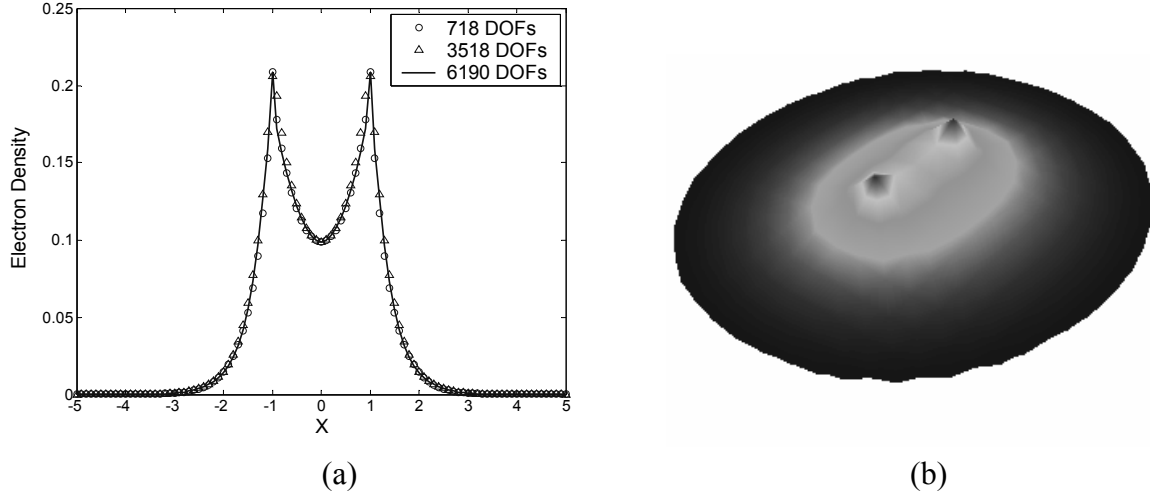(a)   (b)

Figure 11. Electron density distribution of Hydrogen molecular ion obtained by OHPC: (a) Electron density along the x-axis (y=0,z=0)   (b) Electron density contour on x-y plane (z=0)

(3). Hydrogen molecule

This quantum system contains 2 electrons, and thus Kohn-Sham Schrödinger equation based on the density function theory is employed. The electron density field is calculated by the Kohn-Sham wave functions (7), and the effective potential is obtained by (12). Since the effective potential function of DFT based Kohn-Sham Schrödinger equation is dependent on the electron density, a Newton iteration with tolerance $\left\| \rho^n - \rho^{n+1} \right\| < 10^{-10}$ is used, where ρ^n is the electron density solution at the n-th iteration. HSCNI with 8th order Gauss quadrature rule is employed in a small region with dimension of 6 a.u. in each direction, and 2nd order Gauss quadrature rule is used for the rest of the domain.

22

Due to the structure of this quantum system (Figure 7 (c)) that contains 2 nuclei, we compare several forms of intrinsic and extrinsic enrichments as shown in Table 3. For both HPC and OHPC methods, the extrinsic enrichment is employed only near the nuclei $|x_i| \leq 3$ a.u . The HPC and OHPC solutions are also compared with Gaussian-FEM that combines Gaussian orbital function with FEM approximation [55] in Table 3. The results show that OHPC with orbital and monomial bases performs much better than HPC with pure intrinsic or pure extrinsic monomial enrichment. It is also shown that using orbital functions as intrinsic functions and monomials as extrinsic functions yields a slightly better solution compared to the case using orbital functions as extrinsic functions and monomials as intrinsic functions. Both methods consume about the same CPU since the later requires inversion of a 4x4 moment matrix in the intrinsic enrichment. Figure 12 shows the electron density distribution $\rho = \Psi^2$ obtained by the proposed OHPC method.

Table 3   Numerical error of the first level energy for Hydrogen molecule (The reference energy is -1.8479 a.u. [53])

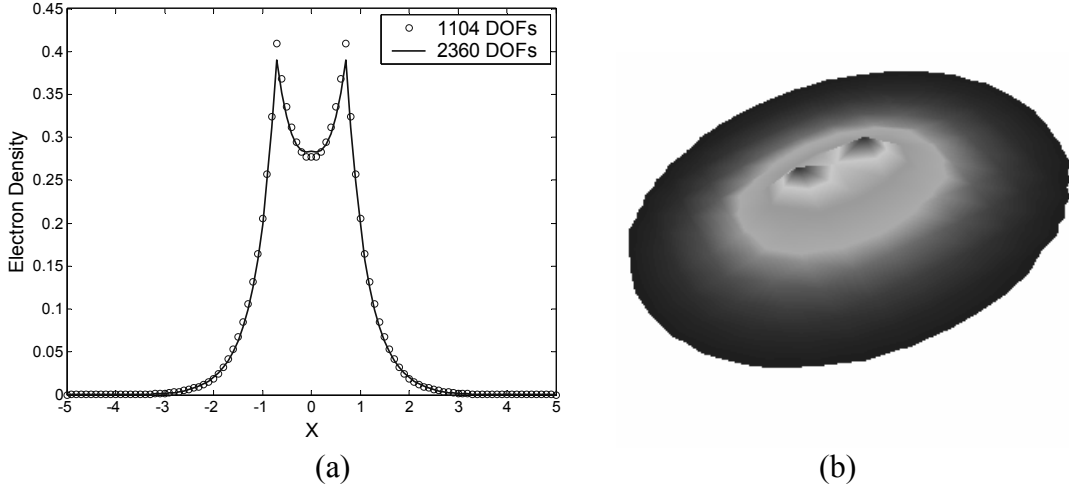| Numerical Methods	No. of nodes	DOFs	Error of the first level energy
Gaussian-FEM [55]	12,167	12,167	0.355%
HPC with intrinsic monomial enrichment $\mathbf{h}_I^{in} = \left[1, \dfrac{x_1 - x_{1I}}{c_1}, \dfrac{x_2 - x_{2I}}{c_2}, \dfrac{x_3 - x_{3I}}{c_3} \right]$	1,331	1,331	1.08%
$\mathbf{h}_I^{ex} = [1]$	9,261	9,261	0.42%
HPC with extrinsic monomial enrichment $\mathbf{h}_I^{in} = [1]$	1,331	2,360	3.51%
$\mathbf{h}_I^{ex} = \begin{cases} \left[1, \dfrac{x_1 - x_{1I}}{c_1}, \dfrac{x_2 - x_{2I}}{c_2}, \dfrac{x_3 - x_{3I}}{c_3} \right], & |x_i| \leq 3 \,\text{a.u.} \\ [1], & |x_i| > 3 \,\text{a.u.} \end{cases}$	2,197	4,384	0.52%
OHPC $\mathbf{h}_I^{in} = \left[1, \dfrac{x_1 - x_{1I}}{c_1}, \dfrac{x_2 - x_{2I}}{c_2}, \dfrac{x_3 - x_{3I}}{c_3} \right]$	729	979	1.03%
$\mathbf{h}_I^{ex} = \begin{cases} \left[1, e^{-r_1}, e^{-r_2} \right], & |x_i| \leq 3 \,\text{a.u.} \\ [1], & |x_i| > 3 \,\text{a.u.} \end{cases}$	1,331	2,017	0.27%
OHPC $\mathbf{h}_I^{in} = \left[1, e^{-r_1}, e^{-r_2} \right]$	729	1,104	0.29%
$\mathbf{h}_I^{ex} = \begin{cases} \left[1, \dfrac{x_1 - x_{1I}}{c_1}, \dfrac{x_2 - x_{2I}}{c_2}, \dfrac{x_3 - x_{3I}}{c_3} \right], & |x_i| \leq 3 \,\text{a.u.} \\ [1], & |x_i| > 3 \,\text{a.u.} \end{cases}$	1,331	2,360	0.16%

Figure 12.   Electron density distribution of Hydrogen molecule: (a) Electron density along the x
axis (y=0,z=0)   (b) Electron density contour on x-y plane (z=0)

6. Conclusion

We present an orbital HP-Cloud (OHPC) approximation and higher order stabilized conforming
nodal integration for solving Schrödinger equation in quantum mechanics. In the proposed OHPC
method, orbital basis functions are reproduced everywhere in the domain of quantum system,
while monomial basis functions are introduced as an additional enhancement of orbital basis
functions through extrinsic enrichment to allow varying order of p-refinement. It is shown that
when reproduction of orbital basis functions is enforced in the HP-Cloud approximation as an
intrinsic enrichment, higher order extrinsic monomial enrichment is only needed in the vicinity of
the nuclei. Due to the employment of higher order basis functions in the HP-Cloud
approximation, a higher order stabilized conforming nodal integration (HSCNI) is developed.
HSCNI is a correction of stabilized conforming nodal integration to achieve higher order accuracy
in the domain integration. Enhanced accuracy and higher order convergence rate are achieved
using HSCNI for the proposed OHPC approximation. Several quantum systems have been
analyzed and the results obtained using the proposed method compared favorably to those
obtained using p-adaptive or Gaussian enriched finite element methods.

References

1   Alemany MMG, Jain M, Kronik L, Chelikowsky JR. Real-space pseudopotential method for computing the electronic properties of periodic systems. *Physical Review B* 2004; **69**:075101-075106.

2   Atluri SN, Zhu T. The Meshless Local Petrov-Galerkin (MLPG) Approach for Solving Problems in Elasto-statics. *Computational Mechanics* 2000; **25**:169-179.

3   Babuška I, Ihlenburg F, Paik E, Sauter S. A generalized finite element method for solving the Helmholtz equation in two dimensions with minimal pollution. *Computer Methods in Applied Mechanics and Engineering* 1995; **128**:325-359.

4   Babuška I, Melenk JM. The Partition of Unity Finite Element Method. *International Journal for Numerical Methods in Engineering* 1997; **40**:727-758.

5   Babuška I, Banerjee U, Osborn JE. Survey of meshless and generalized finite element methods: A unified approach. *Acta Numerica* 2003; **12**:1-125.

6   Babuška I, Zhang Z. The partition of unity method for the elastically supported beam. *Computer Methods in Applied Mechanics and Engineering* 1998; **152**:1-18.

7   Beissel S, Belytschko T. Nodal integration of the element-free Galerkin method. *Computer Methods in Applied Mechanics and Engineering* 1996; **139**:49-74.

8   Belytschko T, Krongauz Y, Organ D, Fleming M, Krysl P. Meshless methods: an overview and recent developments. *Computer Methods in Applied Mechanics and Engineering, special issue on Meshless Methods* 1996; **139**:3-47.

9   Belytschko T, Lu YY, Gu L. Element-free Galerkin methods. *International Journal for Numerical Methods in Engineering* 1994; **37**:229-256.

10   Belytschko T, Lu YY, Gu L. Crack propagation by Element-free Galerkin Methods. *Engineering Fracture Mechanics* 1995; **51**:295-315.

11   Belytschko T, Lu YY, Gu L. Element-free Galerkin Methods for Static and Dynamic Fracture. *Interntional Journal of Solids and Structures* 1995; **32**:2547-2570.

12   Bonet J, Kulasegaram S. Correction and stabilization of smooth particle hydrodynamics methods with applications in metal forming simulation. *International Journal for Numerical Methods in Engineering* 1999; **47**:1189-1214.

13   Bransden BH, Joachain CJ. Quantum Mechanics. Prentice Hall 2000.

14   Chelikowsky JR, Troullier N, Saad Y. Finite-difference-pseudopotential method: Electronic structure calculations without a basis. *Physical Review Letter* 1994; **72**:1240-1243.

15   Chelikowsky JR, Troullier N, Wu K, Saad Y. Higher-order finite-difference pseudopotential method: An application to diatomic molecules. *Physical Review B* 1994; **50**:11355-11364.

16   Chen JS, Pan C, Wu CT, Liu WK. Reproducing Kernel Particle Methods for Large Deformation Analysis of Nonlinear Structures. *Computer Methods in Applied Mechanics and Engineering* 1996; **139**:195-227.

17   Chen JS, Wu CT, Yoon S, You Y. A Stabilized Conforming Nodal Integration for Galerkin Meshfree Methods. *International Journal for Numerical Methods in Engineering* 2001; **50**:435-466.

18   Chen JS, Wu CT, Yoon S, You Y. Nonlinear Version of Stabilized Conforming Nodal Integration for Galerkin Meshfree Methods. *International Journal for Numerical Methods in Engineering* 2002; **53**:2587-2615.

19   De S, Bathe KJ. The Method of Finite Spheres. *Computational Mechanics* 2000; **25**:329-345.

20   Dolbow J, Belytschko T. Numerical integration of Galerkin weak form in meshfree methods. *Computational Mechanics* 1999; **23**:219-230.

21   Duarte CAM, Babuška I, Oden JT. Generalized Finite Element Methods for Three Dimensional Structural Mechanics Problems. *Computers and Structures* 2000; **77**:215-232.

22   Duarte CAM, Oden JT. An h-p adaptive method using clouds. *Computer Methods in Applied Mechanics and Engineering* 1996; **139**:237-262.

23   Duarte CAM, Oden JT. Hp Clouds--an hp Meshless Method. *Numerical Methods for Partial Differential Equations* 1996; **12**:673-705.

24   Garcia O, Fancello EA, Barcellos CS, Duarte CAM. Hp-Clouds in Mindlin's Thick Plate Model. *International Journal for Numerical Methods in Engineering* 2000; **47**:1381-1400.

25   Gingold RA, Monaghan JJ. Smoothed Particle Hydrodynamics: Theory and Application to Non-spherical Stars. *Monthly Notices of the Royal Astronomical Society* 1977; **181**:375-389.

26   Hehre WJ, Radom L, Schleyer P, Pople JA. Ab Initio Molecular Orbital Theory. John Willey & Sons, New York 1986.

27   Heinemann D, Fricke B, Kolb D. Solution of the Hartree-Fock-Slater equations for diatomic molecules by the finite-element method. *Physical Review A* 1988; **38**:4994-5001.

28   Hermansson B, Yevick D. Finite-element approach to band-structure analysis. *Physical Review B* 1986; **33**:7241-7242.

29   Ihm J, Zunger A, Cohen ML. Momentum-space formalism for the total energy of solids. *Journal of Physics C: Solid State Physics* 1979; **12**:4409-4422.

30   Kohn W, Sham LJ. Self-Consistent Equations Including Exchange and Correlation. *Physical Review* 1965; **140**:A1133-1138.

31   Lancaster P, Salkauskas K. Surfaces generated by moving least square method. *Mathematics of Computation* 1981; **37**:141-158.

32   Liszka TJ, Duarte CAM, Tworzydlo WW. Hp-Meshless Cloud Method. *Computer Methods in Applied Mechanics and Engineering* 1996; **139**:263-288.

33   Liu WK, Jun S, Zhang YF. Reproducing Kernel Particle Method. *International Journal for Numerical Methods in Fluids* 1995; **20**:1081-1106.

34   Melenk JM. On generalized finite element methods. Ph.D. dissertation, University of Maryland, College Park, MD 1995.

35   Melenk JM, Babuška I. The partition of unity finite element method: Basic theory and applications. *Computer Methods in Applied Mechanics and Engineering* 1996; **139**:289-314.

36   Melenk JM, Babuška I. Approximation with Harmonic and generalized harmonic polynomial in the partition of unity method. *Computer Assisted Mechanics and Engineering Sciences* 1997; **4**:607-632.

37   Mendonca PT, Barcellos CS, Duarte CAM. Investigations on the Hp-Cloud Method by Solving Timoshenko Beam Problems. *Computational Mechanics* 2000; **25**:286-295.

38   Möes N, Dolbow J, Belytschko T. A finite element method for crack growth without remeshing. *International Journal for Numerical Methods in Engineering* 1999; **46**:131-150.

39   Nayroles B, Touzot G, Villon P. Generalizing the Finite Element Method: Diffuse Approximation and Diffuse Elements. *Computational Mechanics* 1992; **10**:307-318.

40   Oden JT, Duarte CAM, Zienkiewicz OC. A New Cloud-Based hp Finite Element Method. *Computer Methods in Applied Mechanics and Engineering* 1998; **153**:117-126.

41   Oñate E, Idelsohn S, Zienkiewicz OC, Taylor RL. A Finite Point Method in Computational Mechanics: Applications to Convective Transport and Fluid. *International Journal for Numerical Methods in Engineering* 1996; **39**:3839-3866.

42 Parr RG, Yang W. Density Functional Theory of atoms and molecules. Oxford University Press, New York 1989.

43 Pask JE, Sterne PA. Real-space formulation of the electrostatic potential and total energy of solids. *Physical Review B* 2005; **71**:113101-113104.

44 Pickett WE. Pseudopotential methods in condensed matter applications. *Computer Physics Reports* 1989; **9**:115-197.

45 Randles PW, Libersky LD, Petschek AG. On neighbors, derivatives, and viscosity in particle codes. *Proceeding of ECCM Conference*, Munich, Germany, 31 August-3 September 1999.

46 Sukumar N, Moran B, Belytschko T. The Natural Element Method in Solid Mechanics. *International Journal for Numerical Methods in Engineering* 1998; **43**:839-887.

47 Sulsky D, Chen Z, Schreyer HL. A Particle Method for History-Dependent Materials. *Computer Methods in Applied Mechanics and Engineering* 1994; **118**:179-196.

48 Szabo A, Ostlund NS. Modern Quantum Chemistry: Introduction to Advanced Electronic Structure Theory. McGraw-Hill, New York 1989.

49 Tsuchida E, Tsukada M. Electronic-structure calculations based on the finite-element method. *Physical Review B* 1995; **52**:5573-5578.

50 Tsuchida E, Tsukada M. Adaptive finite-element method for electronic-structure calculations. *Physical Review B* 1996; **54**:7602-7605.

51 Tsuchida E, Tsukada M. Large-scale electronic-structure calculations based on the adaptive finite-element method. *Journal of the Physical Society of Japan* 1998; **67**:3844-3858.

52 Wang D, Chen JS, Sun L. Homogenization of Magnetostrictive Particle-Filled Elastomers Using An Interface-enriched Reproducing Kernel Particle Method. *Journal of Finite Element Analysis and Design* 2003; **39/8**:765-782.

53 White SR, Wilkins JW, Teter MP. Finite-element method for electronic structure. *Physical Review B* 1989; **39**:5819-5833.

54 Yamakawa S, Hyodo S. Electronic state calculation of hydrogen in metal clusters based on Gaussian-FEM mixed basis function. *Journal of Alloys and Compounds* 2003; **231**:356-357.

55 Yamakawa S, Hyodo S. Gaussian finite-element mixed-basis method for electronic structure calculations. *Physical Review B* 2005; **71**:035113-035121.

56 You Y, Chen JS, Lu H. Filter, Reproducing Kernel, and Adaptive Meshfree Methods. *Computational Mechanics* 2003; **31**:316-326.